J. Biochem. 2009;145(2)137–150
doi:10.1093/jb/mvn151

The Role of Actomyosin Contractility in the Formation and Dynamics of Actin Bundles During Fibroblast Spreading

Yosuke Senju* and Hidetake Miyata
Department of Physics, Graduate School of Science, Tohoku University, Sendai, Miyagi 980-8578, Japan

Received October 13, 2008; accepted October 22, 2008; published online November 13, 2008

We studied the process of formation of stress fibres and involvement of phosphorylation of myosin-II during spreading of Swiss 3T3 fibroblasts. In cells that were allowed to spread for 1 h on a glass surface, circular bundles of actin and myosin-II filament were present. At 2–3 h after the plating, cells showed a polygonal and polarized shape. The proportion of the cells having circular bundles was decreased, whereas that of the cells with straight bundles of actin filaments was increased. At 4 h after the plating, cells were completely polarized and stress fibres were present at the periphery and the dorsal and ventral surfaces of the cells. Thus, spreading cells possessed different forms of actomyosin bundles corresponding to the cell shape. In circular bundles and stress fibres, myosin regulatory light chains were diphosphorylated. Formation of circular bundles and stress fibres was suppressed after the treatment of the cells with Y-27632, a Rho-kinase inhibitor, or blebbistatin, a myosin-II inhibitor. In digitonin-extracted cells, circular bundles as well as stress fibres contracted following the addition of Mg-ATP. These results suggest that circular bundles are contractile structures containing actin and phosphorylated myosin-II filaments, and the formation of circular bundles is regulated by Rho-kinase.

Key words: actin, adhesion, dynamics, myosin, polarity.

Abbreviations: GFP, green fluorescent protein; MLCK, myosin light chain kinase; MRLC, myosin regulatory light chains; 1P-MRLC, monophosphorylated MRLC; 2P-MRLC, diphosphorylated MRLC; TIRF, total internal reflection fluorescence.

Stress fibres are bundles of actin filaments containing a number of actin-binding proteins such as myosin-II (*1*, *2*), α-actinin (*1*, *3*, *4*) and tropomyosin (*5*). Their ends are linked to focal adhesions that mediate cell-to-substrate contacts and contain clustered integrin and other focal adhesion proteins such as vinculin. As a result of the interaction between F-actin and myosin-II, stress fibres generate a contractile force that is used in cell locomotion and control of cell shape. Recent studies have shown that stress fibres are truly myosin-dependent contractile structures both *in vitro* (*6*, *7*) and *in vivo* (*8*).

There are several different types of actin bundles (*9*). One type is called dorsal stress fibres, which are actin filament bundles crosslinked by α-actinin and do not contain myosin-II at the very end (*2*). Formation of dorsal stress fibres results from mDia1-dependent elongation of actin filaments at focal adhesions followed by bundling by α-actinin. In motile cells, typical stress fibres are formed as a result of the connection of dorsal stress fibres and arcs, which are another type of actin bundles formed at the base of lamellipodia (*10*, *11*). The arcs contain myosin-II (*2*, *9*, *12*) and α-actinin, and show myosin-II dependent dynamics (*13*, *14*).

Activation of myosin-II ATPase by actin has been assumed to cause contraction of stress fibres. The contractile activity depends on the interaction between F-actin and myosin-II, and we have designated it hereafter as 'contractility'. In this process, myosin regulatory light chains (MRLC) have to be mono- or diphosphorylated that is mediated by Rho-kinase (*15*) and myosin light chain kinase (MLCK) (*16*). Rho-kinase also inhibits MRLC phosphatase activity by phosphorylating myosin-binding subunit (*17*, *18*). The resulting loss of phosphatase activity shifts the balance of phosphorylation/dephosphorylation and raises the level of MRLC phosphorylation.

In spreading fibroblasts, stress fibres are initially absent; instead, circular bundles of F-actin are formed (*19*). A previous study has suggested that circular bundles were organized from arcs, which were based on the observation of fixed cells (*20*). Although circular bundles contain myosin-II and resemble stress fibres, the contractility of circular bundles and its role in the formation and dynamics of circular bundles in live cells have not been well understood. In addition, the relationship between circular bundles and stress fibres in cell spreading has remained unclear. We hypothesized that circular bundles are organized in a myosin-II-dependent manner and that their contractility regulates cell shape and the formation of focal adhesions in the spreading process. To evaluate these hypotheses, we observed the dynamics of actin bundles in spreading Swiss 3T3

*To whom correspondence should be addressed. Tel: +81-22-795-6465, Fax: +81-22-795-6774,
E-mail: yosuke@bio.phys.tohoku.ac.jp

fibroblasts using immunofluorescence and time-lapse imaging of green fluorescent protein (GFP)-actin in living cells by epifluorescence and total internal reflection fluorescence (TIRF) microscopy.

MATERIALS AND METHODS

Cell Culture—Swiss 3T3 and Hs68 fibroblasts were used in this study. Cells were cultured in a Petri dish (Greiner, Germany) in Dulbecco's modified Eagle's medium (Nissui, Tokyo, Japan) supplemented with 10% fetal bovine serum (Moregate, Bulimbra, Australia). Cells were maintained at 37°C and at 5% CO_2 in a humidified incubator.

Before the experiments, cells were grown to confluence and dissociated with 0.25% trypsin and 1 mM EDTA (GIBCO, Rockville, MD). Cells were then replated in an observation chamber (*21*) and incubated for an appropriate time.

Antibodies—Anti-vinculin and anti-α-actinin antibodies were from Sigma (St Louis, MO). Anti-β_3 integrin antibody was purchased from Pharmingen (San Diego, CA). Anti-MRLC and anti-monophosphorylated MRLC (1P-MRLC) antibodies were from Cell Signaling Technology, Inc (Beverly, MA). Anti-diphosphorylated MRLC (2P-MRLC) antibodies were from Santa Cruz Biotechnology, Inc (Santa Cruz, CA) and Cell Signaling Technology, Inc. Alexa 488-conjugated goat anti-mouse and Alexa 546-conjugated goat anti-hamster secondary antibodies were from Molecular Probes, Inc (Eugene, OR).

Transfection of GFP-Actin into Swiss 3T3 Fibroblasts—Plasmid encoding GFP-actin was from Clontech (Palo Alto, CA). This plasmid was transfected into Swiss 3T3 cells with Superfect (Qiagen, Hilden, Germany) according to the manufacturer's instructions. After the cells were seeded in the observation chamber, the medium was covered with mineral oil (Sigma). Cells were then observed under a fluorescence microscope. During the observation, the temperature of the chamber was maintained at 37°C, and exposure to the light was kept minimized to prevent photo bleaching.

Inhibitors—Rho-kinase inhibitor Y-27632 (*22*), MLCK inhibitors ML-7 and ML-9 (*23*) were obtained from Calbiochem (La Jolla, CA). An inhibitor of nonmuscle myosin-II (-)-blebbistatin (*24*) was from Sigma. Photoinactivation and phototoxicity of blebbistatin have been reported (*25*, *26*), and so we used Y-27632 as a myosin-II inhibitor for live cell imaging.

SDS–PAGE and Immunoblotting—SDS gel electrophoresis and blotting were performed as previously reported (*27*). Initially, cells were incubated in the medium containing 10 μM Y-27632 or 10 μM ML-7 for an appropriate time. Then, the culture medium was removed and the cells were incubated with ice-cold 10% trichloroacetic acid and 10 mM DTT. Cells were scraped and washed with acetone-containing 10 mM DTT and solubilized in SDS sample buffer, and then the protein concentration was determined. After boiling, cell lysates were electrophoresed on polyacrylamide gels (*28*), and proteins were transferred to a polyvinylidene difluoride membrane using a blotting apparatus (Trans-Blot, Biorad, Hercules, CA). The membrane was blocked and incubated with an antibody against MRLC, 1P-MRLC or 2P-MLRC followed by washing and incubation with horseradish peroxidase-conjugated secondary antibody (GE Healthcare, UK). The bands were visualized with 3,3′-diaminobenzidine.

Contraction Assay—Contraction assay of permeabilized cells was carried out as previously described (*6*, *29*, *30*) with some modifications. Swiss 3T3 and Hs68 fibroblasts were seeded in an observation chamber and incubated for 1 h or 4 h in the case of Swiss 3T3 cells and 2 h or 8 h in the case of Hs68 cells. Then, permeabilization was performed with 0.01% digitonin (Sigma) in an extraction buffer (10 mM imidazole, 100 mM KCl and 2 mM EGTA; 1 μg/ml leupeptin, 1 μg/ml pepstatin and 1 mM DTT; pH 7.2) for 1 min with 0.1 μM tetramethylrhodamine isothiocyanate (TRITC)-phalloidin (Sigma). After washing with the extraction buffer, cells were used in the contraction experiment, which was carried out in a buffer containing 10 mM imidazole, 100 mM KCl, 0.1 mM $CaCl_2$ and 3 mM $MgCl_2$ (pH 7.0 at 22°C). Contraction was initiated by the addition of 0.1 mM Mg-ATP. As described in the 'Results' section, circular bundles and stress fibres in Swiss 3T3 cells were contracted, but the degree of contraction was less than that of Hs68 fibroblasts. For this reason, the results obtained for Hs68 fibroblasts are presented here. The contraction of circular bundles and stress fibres was analysed as follows: in the case of circular bundles, its diameter was measured and in the case of stress fibres, the end-to-end distance was measured. The change in length was presented as 100× (length after ATP perfusion)/(original length) at each time point in both cases.

Immunofluorescence Microscopy—Immunofluorescence microscopy was carried out according to the previously described method (*31*). Fixation was performed with 3% formaldehyde (Sigma) in a buffer containing 5 mM KCl, 137 mM NaCl, 4 mM $NaHCO_3$, 0.4 mM KH_2PO_4, 1.1 mM Na_2HPO_4, 2 mM $MgCl_2$, 5 mM piperazine-1, 4-*bis*(2-ethanesulfonic acid) (pH 6.1), 2 mM EGTA and 5.5 mM glucose (cytoskeleton stabilization buffer) (*32*) at room temperature for 30 min followed by 0.1 M glycine to quench free aldehydes; permeabilization was carried out with 0.2% Triton X-100 (Sigma) for 5 min; blocking was with 1% BSA at room temperature for 20 min. Incubation with the primary antibody was carried out for 1 h, followed by incubation with a suitable secondary antibody. For staining of F-actin, samples were incubated with 0.1 μM TRITC-phalloidin.

Cells were observed under an inverted fluorescence microscope (Axiovert S100, Carl Zeiss, Germany). Cell images were acquired with a cooled charge-coupled device camera (model C4742-95-12ERG; Hamamatsu Photonics, Hamamatsu, Japan) and stored on a hard disk for later analysis.

TIRF microscopy was carried out as described (*21*). Blue (BCL-015, Crystalaser, Reno, NV) or green (DPSS532, Coherent, CA) laser was used as light source. A 63× oil immersion lens (NA 1.25, Carl Zeiss, Germany) and a 40× oil immersion lens (NA 1.30, Carl Zeiss, Germany) were used for observation.

Morphological Analysis—The area and the perimeter of the cell, which were defined for the image projected on

the *x–y* plane, were measured using ImageJ version 1.3 software for epifluorescence images of cells in which the actin filaments were stained. The form factors of individual cells were calculated as $4\Pi S/L^2$, where S is the projected cell area and L is the cell perimeter. This index reflects the irregularity of cell shape: a perfectly round cell has a value of one, and a stellate cell has a value lower than one (*33*). Data were presented as mean ± SD. *F*-test was performed to evaluate the equality of variances, and statistical analyses were made using Student's *t*-test for data sets with equal variance or Welch's *t*-test for data sets with unequal variance.

RESULTS

Change in the Structure and Distribution of Actin Filaments and Alteration of Cell Morphology During Cell Spreading—To investigate the distribution of F-actin bundles during spreading, we fixed Swiss 3T3 fibroblasts and stained for F-actin (Fig. 1A). Cells had been allowed to spread for the period shown in each panel. Initially, there was no distinctive actin filament structure, but at 1 h after the plating, F-actin formed circular bundles (arrowhead) (*19*). At 2 h after the plating, some cells possessed straight bundles of actin filament, whereas others still had circular bundles. At 4 h after the plating, most of the cells possessed straight actin bundles (arrows) that were found to be stress fibres (see below). Thus, F-actin formed circular bundles in early stages of cell spreading.

The above observation of the behaviour of F-actin during spreading (Fig. 1A) suggested that the morphology of F-actin bundles changed with the size and shape of the cell: the shape of the cell possessing circular bundles appeared to be round and that of the cell possessing stress fibres seemed to be polygonal. Therefore, we analysed cell morphology quantitatively (Fig. 1B). The cell area increased until 2 h after the plating; but beyond this time point, the increase ceased. The values of the form factor were relatively high in the early stages of cell spreading, indicating that the cells were round. Then, it decreased during spreading, reflecting a gradual cell shape change from round to polygonal. However, unlike the change in cell size, the transformation continued until 8 h. The proportion of the cells possessing circular bundles exhibited a similar tendency as the form factor. These results collectively suggest that the loss of circular bundles and the change in cell shape are interrelated phenomena.

Formation of Circular Bundles from Arcs and Their Dynamics—Although studies concerning stress fibres have been frequent, the manner in which circular bundles of F-actin are formed remains unclear. Therefore, we observed Swiss 3T3 fibroblasts expressing GFP-actin (Fig. 2A): this cell had been allowed to spread for 67 min after the plating. An arc (both ends indicated by arrowheads), which was formed at the cell periphery, elongated and at the same time moved towards the nucleus. The flow velocity was 0.38 ± 0.09 μm/min (mean ± SD, $n = 30$) and the elongation rate was

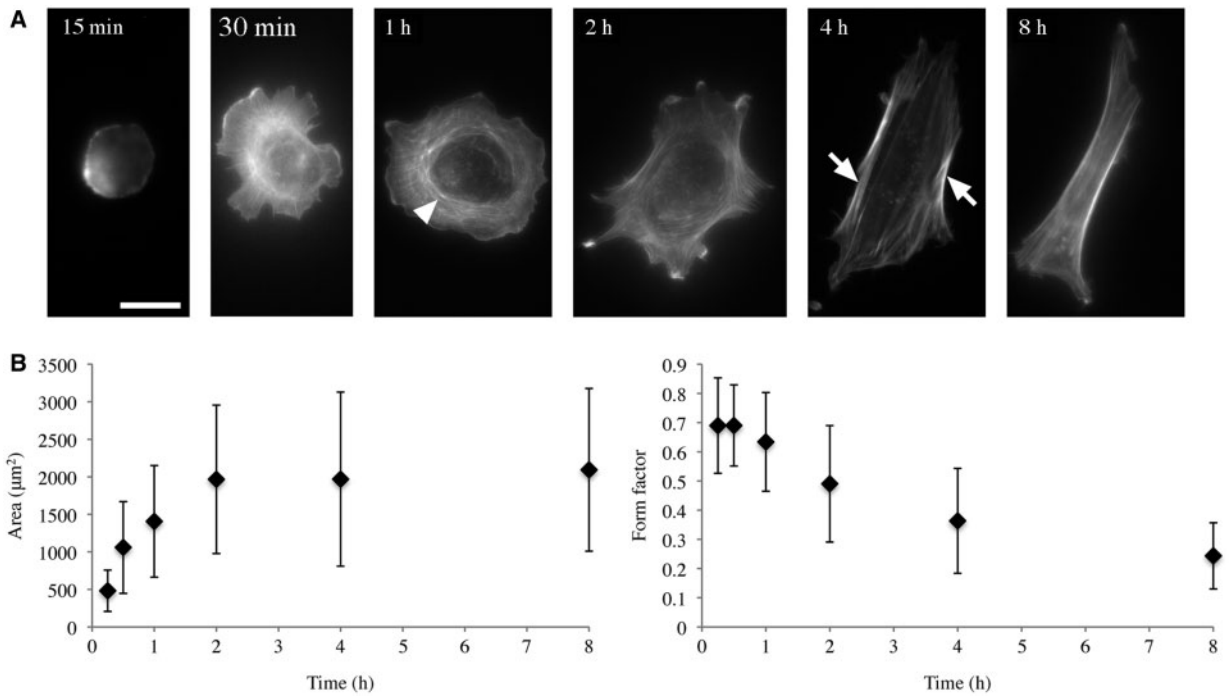

Fig. 1. **Change in the arrangement of F-actin bundles in spreading Swiss 3T3 fibroblasts and the result of morphometry.** (A) Structure and distribution of F-actin bundles observed by epifluorescence microscopy. Cells were fixed at the indicated time after the plating, and F-actin was stained with TRITC-phalloidin. One hour after the plating, F-actin formed circular bundles (arrowhead). At 4 h after the plating, F-actin organized into stress fibres (arrows). Scale bar = 20 μm. (B) Projected cell area and the form factor of spreading cells (mean ± SD, $n = 200$). Form factor is high when the cell shape is round and decreases as the cell shape becomes polygonal.

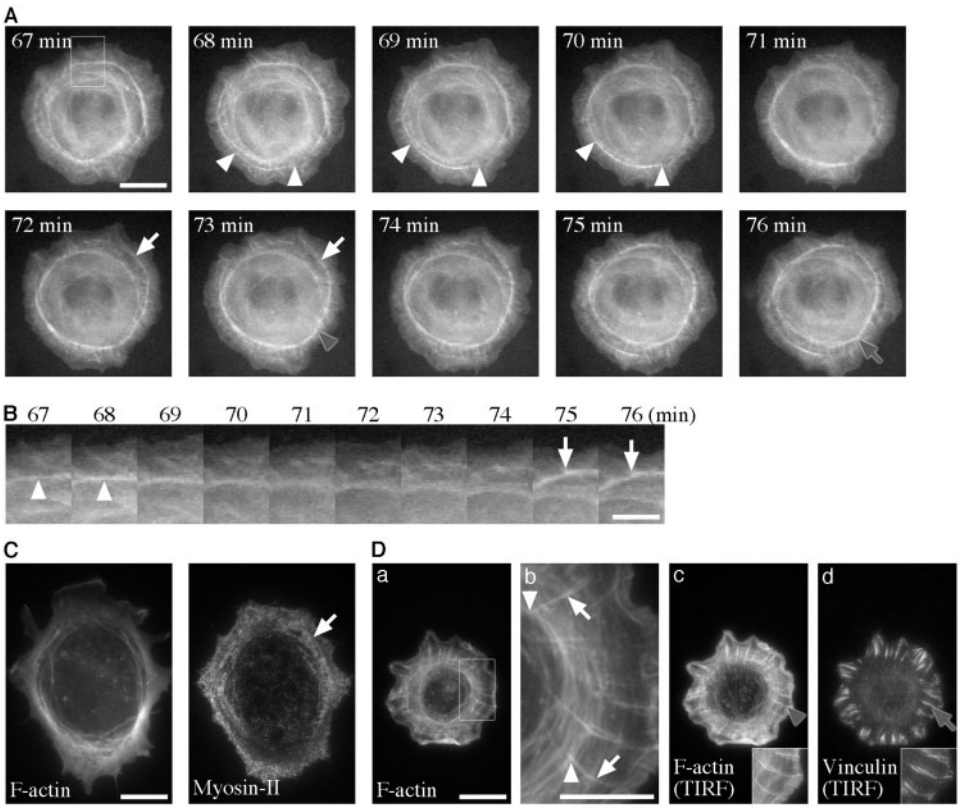

Fig. 2. **Formation and dynamics of circular bundles of F-actin in Swiss 3T3 fibroblasts expressing GFP-actin.** (A) Successive images of Swiss 3T3 fibroblast expressing GFP-actin. The top left panel represents the epifluorescence image at 67 min after the plating. An arc was formed at the cell periphery at 68 min and then underwent elongation (white arrowheads). At 72 min, another arc was formed (white arrow). At 73 min, the two arcs were joined together in the region indicated by grey arrowhead. At 76 min, circular bundles were formed by closure of the joined arcs (grey arrow). Scale bar = 20 μm. (B) Magnified image of the boxed region in (A). An arc was formed at the cell periphery (arrowhead) moved in the downward direction towards the nucleus. At 75 min, a new arc (arrow) was formed and moved in the same direction. Scale bar = 10 μm. (C) Epifluorescence images of stained F-actin (left panel) and myosin-II (right panel) showed localization of myosin-II along circular bundles (arrow). Scale bar = 20 μm. D: (a) Epifluorescence image of a Swiss 3T3 fibroblast had been allowed to spread for 1 h and then fixed and stained for F-actin. Scale bar = 20 μm. (b) Boxed region in (a) is magnified. Circular bundles (arrowheads) are associated with dorsal stress fibres (arrows). Scale bar = 10 μm. (c) Fluorescence staining of F-actin in the same cell was observed by TIRF microscopy. The inset shows a magnified image of dorsal stress fibres indicated by grey arrowhead. (d) Immunofluorescence staining of vinculin in the same cell was observed by TIRF microscopy. The inset shows a magnified image of vinculin indicated by grey arrow.

1.30 ± 0.18 μm/min (mean ± SD, $n = 6$). Another arc was formed at 72 min (arrows). Then, the two arcs were joined at the position indicated by a grey arrowhead at 73 min. At 76 min, the arcs formed a circle, indicating that they formed a circular bundle (Supplementary Movie 1).

Figure 2B shows the enlarged view of the boxed region in Fig. 2A. An arc was generated at the cell periphery and flowed towards the nucleus (arrowheads). During the process of transport, the vertical position of circular bundles appeared to become higher, because they could only be brought into focus at higher focus levels. This result indicates that circular bundles were translocated along the cytoplasmic side of the apical cell surface.

Stress fibres consist of myosin-II (*1*, *2*), α-actinin (*1*, *3*, *4*) and tropomyosin (*5*) and generate tension in a myosin-II-dependent manner (*8*). We investigated the myosin-II and α-actinin distribution in circular bundles in the cells 1 h after the plating (Fig. 2C). Circular bundles contained myosin-II (arrow) and α-actinin (data not shown), suggesting a role of these proteins as bundling factors. On the other hand, myosin-II was excluded from lamellipodia and existed in lamella as previously reported (*34–37*). Thus, during the process of the flow of the arc from the base of the lamellipodia to the lamella, myosin-II seemed to be incorporated into arcs (*2*).

To elucidate the structural relationship between circular bundles and focal adhesions, we observed the distribution of F-actin and vinculin (Fig. 2D). The left-most panel (a) shows fluorescence staining of F-actin in the cell that had been allowed to spread for 1 h. The boxed region is magnified and shown in (b). As indicated by arrowhead, circular bundles associated with dorsal stress fibres (arrows) oriented in the radial direction. We investigated the process of formation of dorsal stress fibres in the cells expressing GFP-actin by epifluorescence and TIRF microscopy and found that dorsal stress fibres formed at the cell periphery and elongated towards the cell nucleus as in migrating cells (*2*). The elongation rate of dorsal stress fibres before they were bound to the arcs was 0.34 ± 0.15 μm/min (mean ± SD, $n = 30$).

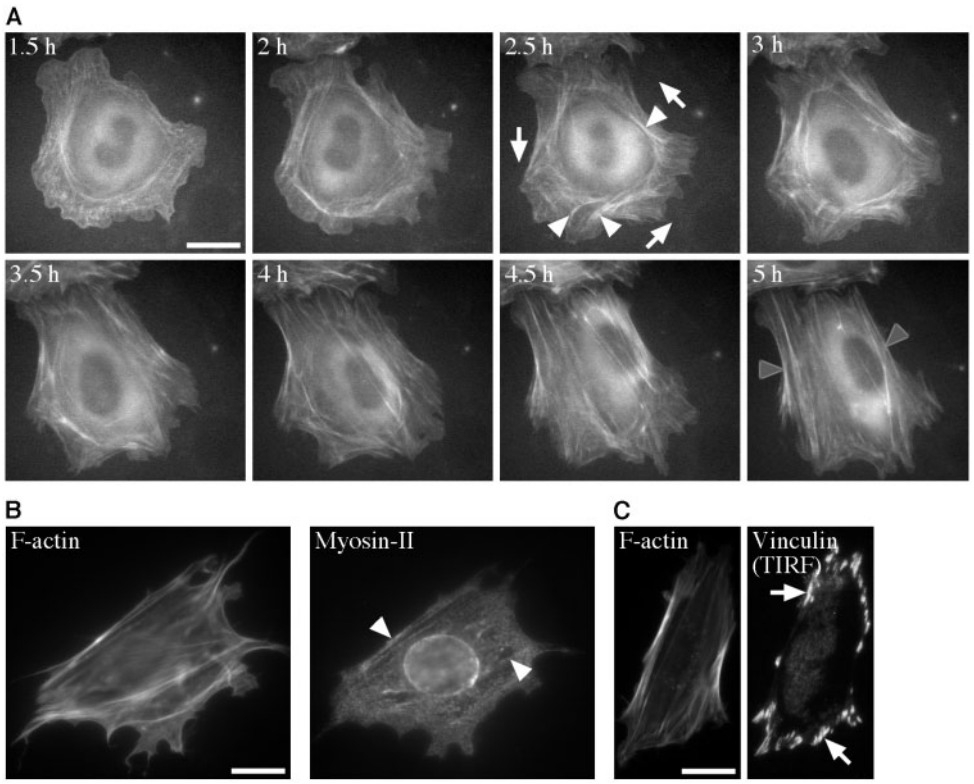

Fig. 3. **Rotation of circular bundles and formation of stress fibres.** (A) A sequence of the epifluorescence images of Swiss 3T3 fibroblast expressing GFP-actin. The top left panel was imaged at 1.5 h after the plating. At 2.5 h, circular bundles ceased to flow and started rotating with dorsal stress fibres (arrowheads) in the direction indicated by arrows. By 5 h, dorsal stress fibres and circular bundles were rearranged into stress fibres (grey arrowheads). Scale bar = 20 μm. (B) Distribution of F-actin (left panel) and myosin-II (right panel) in a fixed cell was observed by epifluorescence microscopy. Myosin-II was localized along stress fibres (arrowheads). Scale bar = 20 μm. (C) Fluorescence staining of F-actin (left panel, epifluorescence) and immunofluorescence staining of vinculin (right panel, TIRF) in another fixed cell. Vinculin-containing adhesions were localized at the ends of stress fibres (arrows). Scale bar = 20 μm.

Thus, it appears that circular bundles were connected to dorsal stress fibres during the process of elongation. At the ends of these dorsal stress fibres (c, grey arrowhead), vinculin (d, grey arrow) was localized, the pattern of which was elongated, as revealed by TIRF microscopy. The β_3 integrin was found to colocalize with vinculin at the ends of the dorsal stress fibres (data not shown), indicating that these structures were focal adhesions (*38*). These observations suggest that circular bundles were linked to the substrate by focal adhesions through dorsal stress fibres.

Rotation of Circular Bundles and Formation of Stress Fibres—To understand the relationship between organized circular bundles and stress fibres, we observed Swiss 3T3 fibroblast expressing GFP-actin: observation was begun at 1.5 h after the plating (Fig. 3A). At 2.5 h after the plating, circular bundles (arrowheads) ceased to flow and began to rotate around the nucleus (direction of rotation is indicated by arrows, Supplementary Movie 2). Both clockwise and counterclockwise rotations were observed in other cells. Similar results have been previously obtained by differential interference contrast microscopy (*39*). We further found that during the rotation (2.5–3.5 h after the plating), circular bundles were disassembled, which was followed by the formation of straight bundles (grey arrowheads at 5 h), and were concomitant with cell polarization. Unlike circular bundles, the straight bundles, once formed, did not show any significant movement.

Figure 3B shows the immunofluorescence staining of myosin-II in Swiss 3T3 fibroblast 4 h after the plating. Myosin-II was concentrated along the straight actin bundles (arrowheads). α-Actinin also localized along these straight bundles (data not shown). Figure 3C shows the immunofluorescence staining of vinculin, which demonstrated that vinculin was localized at the ends of the straight actin bundles (arrows). The β_3 integrin was colocalized with vinculin (data not shown). Therefore, these organized straight F-actin bundles were stress fibres.

Distribution of Phosphorylated MRLC During Fibroblast Spreading—Circular bundles contained myosin-II, and we next examined the state of phosphorylation of MRLC and investigated the possible relation of MRLC phosphorylation to the formation of circular bundles by inhibiting Rho-kinase with Y-27632 (Fig. 4).

Immunofluorescence microscopy demonstrated that, in control cells, 2P-MRLC was colocalized with circular bundles at 1 h after the plating (Fig. 4A, panel c, arrowhead). At 4 h after the plating, 2P-MRLC was found

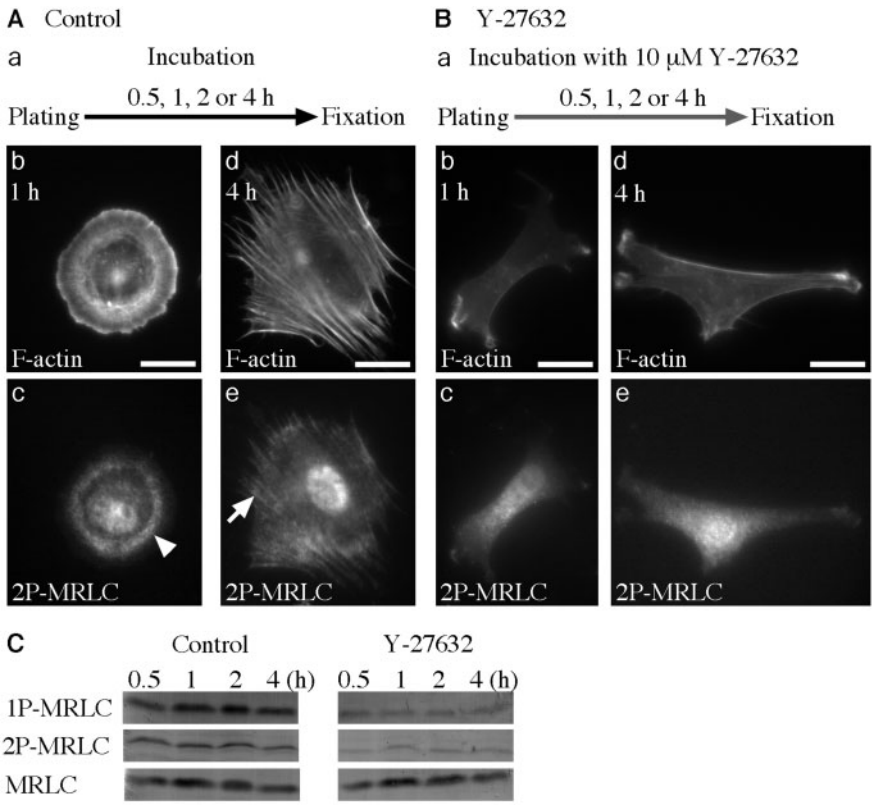

Fig. 4. **Distribution of 2P-MRLC in control and Y-27632-treated cells.** (A) Experimental procedure (a), epifluorescence images of F-actin (b and d) and 2P-MRLC (c and e) in control cells. Immunostaining of 2P-MRLC showed localization along circular bundles at 1 h after the plating (arrowhead). At 4 h, MRLC in stress fibres was diphosphorylated (arrow). Scale bar = 20 μm. (B) Procedure of inhibitor treatment (a), distribution of F-actin (b and d) and 2P-MRLC in Y-27632-treated cells (c and e). Cells were observed by epifluorescence microscopy. Scale bar = 20 μm. (C) Immunoblotting analysis of 1P-MRLC and 2P-MRLC of control and Y-27632-treated cells. Numbers inscribed on the top indicate the time after the plating (0.5, 1, 2 and 4 h).

to colocalize with stress fibres (Fig. 4A, panel e, arrow). 1P-MRLC was also localized at circular bundles and stress fibres (data not shown). Thus, not only stress fibres but also circular bundles contained phosphorylated myosin-II, suggesting that active myosin-II was present in the actin bundles from relatively early stages of spreading. On the other hand, in cells incubated with 10 μM Y-27632 after the plating, the fluorescence intensity of 2P-MRLC (Fig. 4B, panels c and e) was lower than that of control cells (Fig. 4A, panels c and e, respectively) up to 8 h after the plating. Fluorescence intensity of 1P-MRLC was also lower up to 8 h after the plating (data not shown).

In addition to immunofluorescence microscopy, we investigated the level of MRLC phosphorylation by immunoblotting analysis of whole cell lysates (Fig. 4C). In control cells, MRLC was mono- and diphosphorylated at all the time points (0.5, 1, 2 and 4 h). On the other hand, the levels of monophosphorylation and diphosphorylation of MRLC were significantly lower in cells treated with 10 μM Y-27632 at all the time points. This result is consistent with those of previous studies that have shown that Rho-kinase monophosphorylated (*15*) or diphosphorylated (*40*) MRLC. Immunofluorescence and immunoblotting analysis results suggest that the formation of circular bundles depends on the phosphorylation of MRLC by Rho-kinase.

Effects of Inhibition of MRLC Phosphorylation on Focal Adhesions and Cell Morphology—It is known that the formation of stress fibres requires contractility, which is brought about by the phosphorylation of MRLC (*41*). We thus examined how the inhibition of the phosphorylation of MRLC might affect the structure of actin bundles, cell shape and the process of formation of focal adhesions during cell spreading (Fig. 5).

In the presence of 10 μM Y-27632 (Fig. 5A) or 10 μM blebbistatin (Fig. 5B) before the fixation, circular bundles were not formed at 1 h (panel b) and even at 4 h (panel e) after the plating, although thin dorsal stress fibres (panel c, arrowheads) and immature vinculin clusters (panels d and g, white and grey arrows) were revealed by TIRF microscopy. Magnified images (panels d and g) show that vinculin clusters (1 h, white arrows; 4 h, grey arrows) became smaller and rounder than those in the control cells, as shown in Figs 2D and 3C. Thus, the phosphorylation of myosin-II and active interaction between actin and myosin-II is necessary for the formation of circular bundles and development of adhesion structures.

Figure 5A and B also suggest that as a result of the inhibitor treatments, the cell shape became irregular. We also analysed cell morphology (Fig. 5C). In the cells treated with 10 μM Y-27632 or 10 μM blebbistatin,

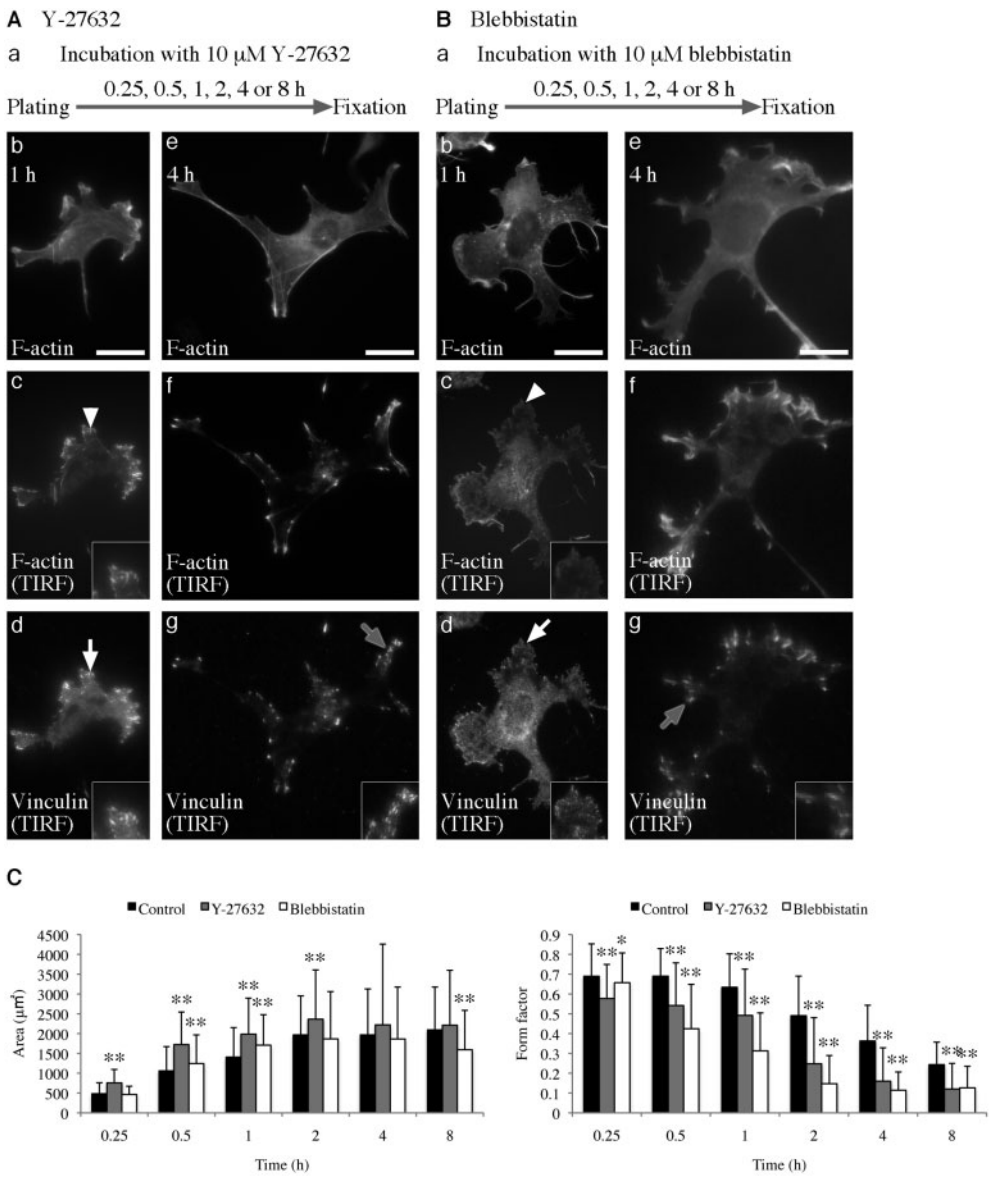

Fig. 5. **Effect of myosin-II inhibitors on the formation of circular bundles.** (A) Experimental procedure (a), epifluorescence images of F-actin in a Swiss 3T3 cell cultured for 1 (b) or 4 h (e) in the presence of 10 μM Y-27632. Circular bundles were not formed at 1 h after the plating. TIRF images of the same cell show that dorsal stress fibres (c, inset shows magnified image of the place indicated by arrowhead) were thinner than those in the control cells with smaller vinculin clusters (d, inset shows magnified image of the place indicated by white arrow) located at their ends. At 4 h after the plating, stress fibres were not observed by epifluorescence (e) and TIRF microscopy (f) and vinculin-containing focal adhesions were smaller than those of the control cells (g, inset shows magnified image of the place indicated by grey arrow) as revealed by TIRF microscopy. Scale bar = 20 μm. (B) Swiss 3T3 cells were cultured in the presence of 10 μM blebbistatin (a). As in the Y-27632-treated cells, circular bundles were not formed at 1 h as shown by epifluorescence microscopy (b). Thinner dorsal stress fibres (c, inset shows magnified image of the place indicated by arrowhead) and smaller vinculin clusters (d, inset shows magnified image of the place indicated by white arrow) were formed as shown by TIRF microscopy. At 4 h after the plating, stress fibres were not organized as shown by epifluorescence (e) and TIRF microscopy (f) and vinculin clusters were immature as shown by TIRF microscopy (g, inset shows magnified image of the place indicated by grey arrow). Scale bar = 20 μm. (C) Left panel, projected area of the control and inhibitor-treated cells (mean ± SD, $n = 200$ for each condition); right panel, form factor (mean ± SD, $n = 200$ for each condition). In the Y-27632-treated cells (grey bar), the cell area was significantly larger than that of the control cells (black bar) at 0.25, 0.5, 1 and 2 h ($^{*}P < 0.05$; $^{**}P < 0.01$), whereas the form factor was lower than that of the control cells at all the time points. In the blebbistatin-treated cells (white bar), the cell area was larger at 0.5 and 1 h and lower at 8 h than that of the control cells. The form factor was significantly lower than that of the control cells at all time points.

the cell areas were larger than those of the control cells particularly at the early stages of spreading (Y-27632: 0.25, 0.5, 1 and 2 h; blebbistatin: 0.5 and 1 h). The reason for a smaller area in blebbistatin-treated cells at 8 h seems to be due to the extremely irregular cell shape. The values of the form factor of the inhibitor-treated cells were significantly lower than those of the control cells at all the time points. Hence, suppression of the formation

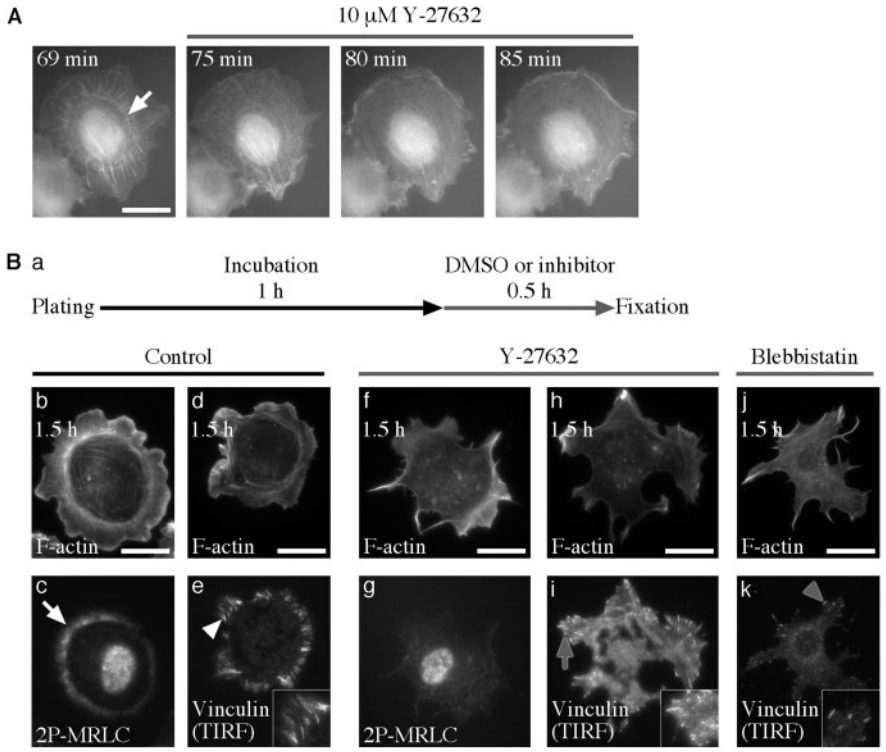

Fig. 6. **Maintenance of the structure of circular bundles was regulated by actomyosin contractility.** (A) Effect of the treatment with Y-27632 on circular bundles in Swiss 3T3 fibroblasts expressing GFP-actin. The cells were observed by epifluorescence microscopy. The leftmost panel shows the cell 69 min after the plating. Circular bundles are indicated by arrows. At 70 min, 10 μM Y-27632 was added. Scale bar = 20 μm. (B) Experimental procedure (a): at 1 h after the plating, Swiss 3T3 fibroblasts were treated with DMSO, 10 μM Y-27632 or 10 μM blebbistatin for 30 min followed by fixation. Cells were then stained for F-actin (b, d, f, h, j: epifluorescence) plus 2P-MRLC (c, g: epifluorescence) or vinculin (e, i, k: TIRF). White arrow in (c) indicates colocalization of 2P-MRLC with organized circular bundles, and white arrowhead in (e) indicates vinculin clusters (inset shows magnified image indicated by white arrowhead) in control cells. Grey arrow in (i) and grey arrowhead in (k) show vinculin-containing adhesions in the Y-27632 and blebbistatin-treated cells, respectively [insets in (j) and (k) shows magnified image of the place indicated by grey arrow and grey arrowhead, respectively]. Scale bar = 20 μm.

of circular bundles resulted in faster spreading in the early stages and a more irregular shape throughout the following stages.

Contractility Is Essential for the Maintenance of the Structure of Circular Bundles—The above experiments have demonstrated that the contractility that depends on the phosphorylation of myosin-II was necessary for the formation of circular bundles. It has been suggested that isometric tension in stress fibres, which develops when the contractile force generated by stress fibres is sustained by adhesions at both ends (*42*), is necessary for the maintenance of the structure of stress fibres (*41*). To elucidate this point with circular bundles, we next examined the inhibitor effect on the organized circular bundles (Fig. 6) in order to examine the role of contractility in the maintenance of the integrity of the structure of circular bundles (hereafter, we have called it 'maintenance' of circular bundles).

Swiss 3T3 fibroblast expressing GFP-actin, which was allowed to spread for 69 min, and which developed circular bundles (Fig. 6A, arrow), was treated with 10 μM Y-27632 at this time point and observed using epifluorescence microscopy. At 85 min, organized circular bundles became difficult to identify and the formation of arcs had ceased (Supplementary Movie 3). This result suggests the necessity of the phosphorylation-dependent contractility for the maintenance of the structure of circular bundles.

To examine the distribution of phosphorylated MRLC and the focal adhesion protein vinculin after the disruption of circular bundles, Swiss 3T3 fibroblasts were allowed to spread for 1 h and then treated with 10 μM Y-27632 or 10 μM blebbistatin for 30 min followed by fixation and immunostaining for 1P-MRLC, 2P-MRLC or vinculin (Fig. 6B, panel a). In the control cells, circular bundles (panel b) colocalized with 2P-MRLC (panel c, arrow) and 1P-MRLC (data not shown). Vinculin clusters were radially elongated (panel e, arrowhead; magnified image in the inset). In the Y-27632-treated cells, circular bundles disappeared (panels f and h), the fluorescence intensity of 2P-MRLC (panel g) significantly decreased and vinculin-containing adhesions became rounder and smaller (panel i, grey arrow; magnified image in the inset) than those of control cells. The fluorescence intensity of 1P-MRLC also decreased (data not shown). In blebbistatin-treated cells, circular bundles diminished (panel j) and vinculin-containing adhesions became rounder and smaller than those of control cells as in

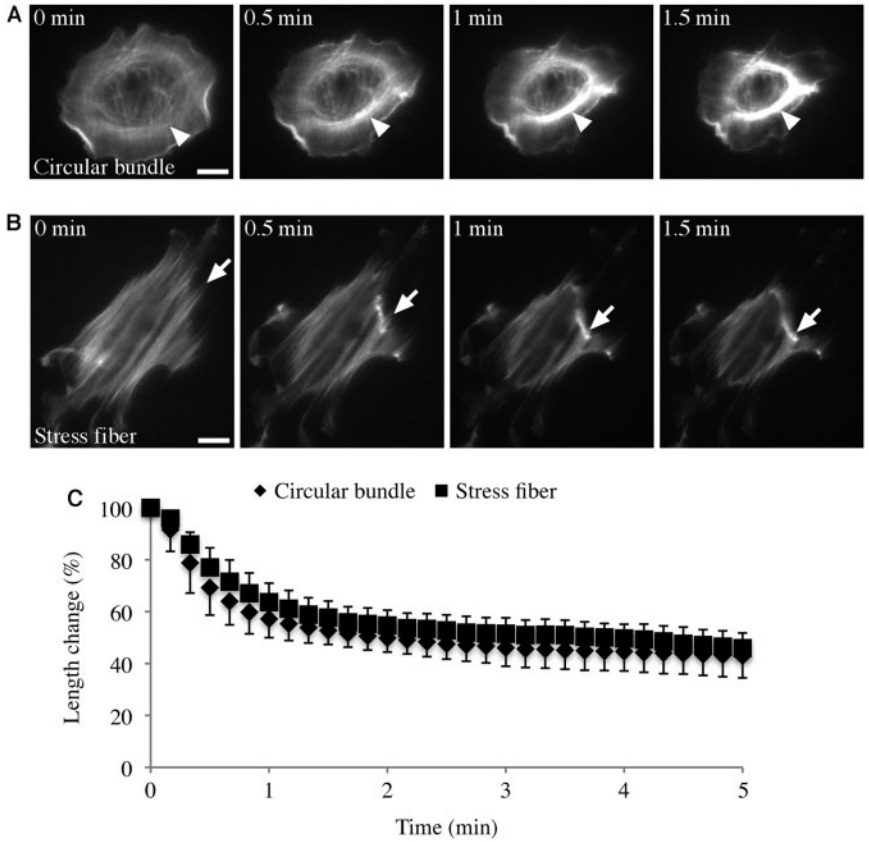

Fig. 7. **Analysis of contractility of actin bundles.** (A) Contraction of circular bundles. Sequential images of Hs68 cell had been allowed to spread for 2 h followed by extraction with digitonin and staining for F-actin. Images were obtained by epifluorescence microscopy. Arrowheads indicate the contraction of circular bundles after perfusion with 0.1 mM Mg-ATP (0 min). Scale bar = 20 μm. (B) Contraction of stress fibres. Hs68 cell had been allowed to spread for 8 h and was processed as mentioned earlier. Arrow indicates one of the contracting stress fibres. C: Time course of the contraction of circular bundles (diamond plots) and stress fibres (square plots), as represented with percent length change.

the Y-27632-treated cells (panel k, grey arrowhead; magnified image in the inset). Thus, even after the cell was spread completely, the inhibition of contractility suppressed the formation of circular bundles and vinculin-containing adhesions.

To investigate the role of organized circular bundles in cell morphology, we compared the area of control cells at 1.5 h after the plating of cells that were allowed to spread for 1 h and further treated with 10 μM Y-27632 or 10 μM blebbistatin for 30 min. In the control cells, the cell area was $1611 \pm 1011\,\mu m^2$ (mean ± SD, $n = 50$). On the other hand, the cell area of the Y-27632-treated cells was $2025 \pm 896\,\mu m^2$ (mean ± SD, $n = 50$) and that of the blebbistatin-treated cells was $1888 \pm 873\,\mu m^2$ (mean ± SD, $n = 50$). Thus, as a result of the inhibition of contractility, circular bundles diminished and the average cell area increased ($P < 0.05$ in the case of Y-27632-treated cells). Thus, the disappearance of circular bundles was accompanied with additional cell spreading.

Circular Bundles Are Contractile—The inhibition experiments and analysis of MRLC phosphorylation suggested that circular bundles as well as stress fibres possess contractility that depends on the phosphorylation of myosin-II. Therefore, we investigated the role of contractility in the formation and maintenance of circular bundles by using a digitonin-permeabilized cell model that is capable of contraction (Fig. 7).

Hs68 fibroblasts that were extracted with digitonin and stained for F-actin were perfused with 0.1 mM Mg-ATP solution (Fig. 7A). Circular bundles (arrowheads) began to contract immediately after the addition of Mg-ATP (Supplementary Movie 4). In the well-spread cells, stress fibres (Fig. 7B, arrows) contracted following the addition of Mg-ATP (Supplementary Movie 5). This contraction did not seem to be due to the depolymerization of F-actin, because the fluorescence intensities per unit area of the region of shortening stress fibres were increasing (arrows). No contraction occurred upon perfusion of the contraction buffer without ATP. Thus, these contractions were ATP dependent. Both types of contraction were almost completed within 5 min after the addition of Mg-ATP.

Figure 7C shows the time courses of the decrease in the length of circular bundles and stress fibres in the digitonin-permeabilized cells. Contraction of circular bundles (diamonds) and that of stress fibres (squares) was biphasic as previously reported (*6*, *43*, *44*). The length of circular bundles decreased to 57.2% ± 7.2% of the original length within 1 min and then gradually

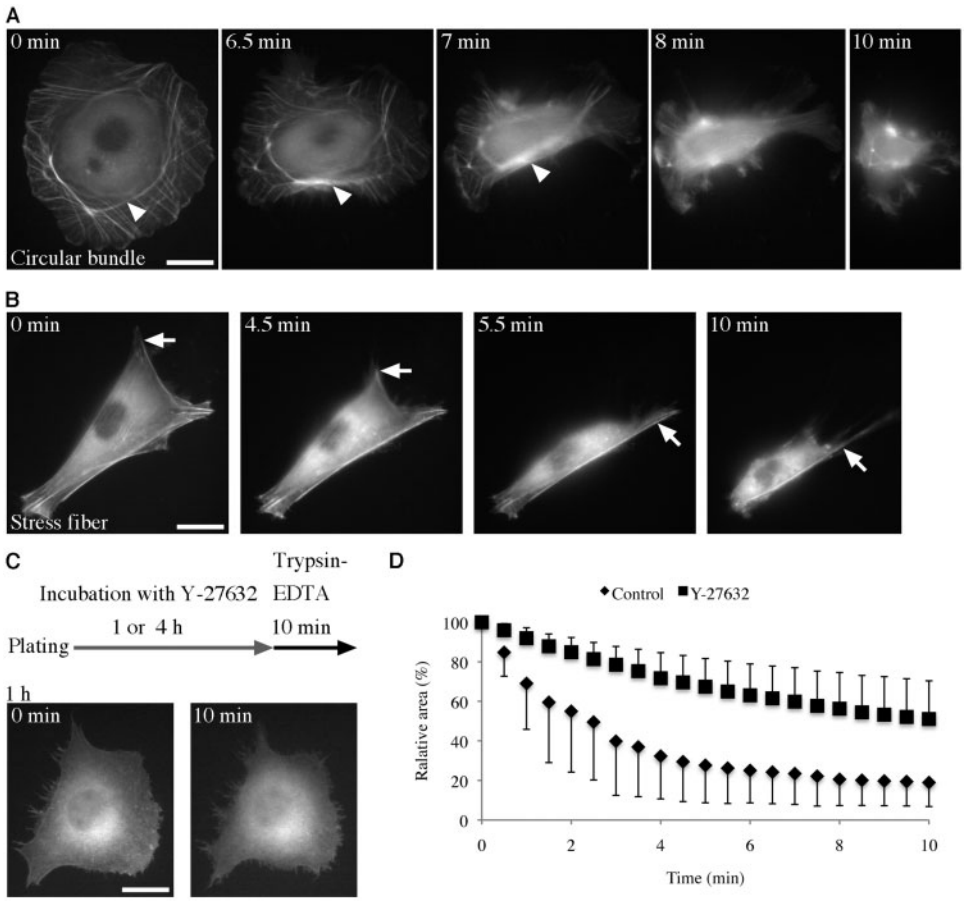

Fig. 8. **Isometric tension is necessary for the maintenance of the structure of circular bundles.** (A) Effect of partial destruction of adhesions on the structure of circular bundles. Swiss 3T3 fibroblasts expressing GFP-actin were allowed to spread for 1 h. Then, 0.05% trypsin-EDTA was perfused at 0 min and the cell was observed by epifluorescence microscopy. The time after the addition of trypsin-EDTA is indicated in each panel. Arrowheads indicate the shape change of circular bundles after trypsinization. Scale bar = 20 μm. (B) Effect of partial destruction of adhesions on stress fibres. Swiss 3T3 fibroblasts expressing GFP-actin were allowed to spread for 4 h, and images were obtained by epifluorescence microscopy. Arrows indicate the contraction of stress fibres after treatment with 0.05% trypsin-EDTA. Scale bar = 20 μm. (C) Trypsinization of Swiss 3T3 fibroblasts expressing GFP-actin after incubation with Y-27632. As shown in the upper schematic diagram, cells were incubated with 10 μM Y-27632 for 1 h or 4 h (data not shown). Then 0.05% trypsin-EDTA was added and observed for 10 min by epifluorescence microscopy. Scale bar = 20 μm. (D) Analysis of the change in the relative area ratios versus initial area of the cells. Control (diamond plots) and Y-27632-treated cells (square plots) were compared 10 min after trypsinization.

decreased to 43.0% ± 8.5% ($n = 8$). Stress fibres contracted to 63.6% ± 7.3% within 1 min and then gradually decreased to 45.9% ± 5.8% ($n = 11$). These results demonstrate that the contractility of actomyosin bundles had developed from early stages of spreading, which is consistent with the presence of phosphorylated MRLC in circular bundles.

Detachment of Focal Adhesions from the Substrate Results in the Disappearance of Circular Bundles—We next examined the role of mechanical tension in the maintenance of the structure of circular bundles and cell retraction: Swiss 3T3 fibroblasts expressing GFP-actin were detached from the substrate with 0.05% trypsin-EDTA in phosphate-buffered saline (Fig. 8).

After the addition of trypsin-EDTA, circular bundles in the cells spreading for 1 h (Fig. 8A, arrowheads) changed their round shape concomitant with the anisotropic retraction of the cell due to the partial destruction of adhesion structures (Supplementary Movie 6). Blurring of the fluorescence image of circular bundles suggests that slackening occurred in circular bundles. Stress fibres in the cell spreading for 4 h (Fig. 8B, arrows) also contracted and diminished with retraction of the cell as previously reported (*45*).

On the other hand, the cell retraction induced by trypsin-EDTA was suppressed by treatment of the cells with 10 μM Y-27632 for 1 (Fig. 8C) or 4 h (data not shown), which inhibited the formation of circular bundles and stress fibres as demonstrated in Figs 4 and 5.

We analysed the areas of the control and inhibitor-treated cells after trypsinization (Fig. 8D). At 1 h after the plating, the relative area of the control cells (diamonds) significantly decreased immediately after the treatment of trypsin-EDTA, then gradually decreased to 18.9% ± 12.1% of the initial area by 10 min ($n = 12$). In the Y-27632-treated cells (squares), however, the cells contracted very slowly only up to 51.1% ± 19.3% ($n = 15$). Similar results were obtained in the case of stress fibres

in the cells 4 h after the plating (control: 18.9% ± 10.8% by 10 min, $n = 13$; Y-27632: 41.7% ± 20.8% by 10 min, $n = 24$). These results suggest the presence of isometric tension in circular bundles that was generated as a result of interaction between phosphorylated myosin-II and actin.

DISCUSSION

Two types of actin structures—circular bundles and stress fibres—and their existence at distinctive stages of cell spreading have been reported (*19*). However, the role of actomyosin contractility in the formation of circular bundles and the relationship between circular bundles and stress fibres in the context of cell spreading has remained unclear. To elucidate these points, we observed the structure and distribution of actin filament bundles, examined the contractility of these structures and attempted to relate these characteristics to cell morphology and adhesions at different stages of cell spreading.

As schematically shown in Fig. 9, our study strongly suggests that circular bundles are organized in an actomyosin-dependent manner and regulated the organization of cell morphology and focal adhesions in the early stages of cell spreading. Our live cell observations confirmed that until 1 h after the plating, the cells were round and that circular bundles were formed from arcs that were generated at the cell periphery (Figs 1B and 2A). Circular bundles were similar to stress fibres in molecular composition; however, as we have demonstrated, cell-to-substrate adhesions were mediated by dorsal stress fibres that were connected to circular bundles at one end and to the substrate at the other end (Fig. 2D). Around 2 h after the plating, the centripetal flow of actin filament bundles stopped and the rotation of circular bundles occurred, which was followed by the disassembly of circular bundles and reorientation of actin bundles, and finally stress fibres were formed with polarization of the cell shape (Fig. 3).

We found that MRLC in circular bundles was diphosphorylated (Fig. 4). Diphosphorylation of MRLC enhances actin-activated myosin-II ATPase activity more strongly than does monophosphorylation (*16*). Thus, circular bundles would have a relatively high contractility. In the Y-27632-treated cells, the levels of mono- and diphosphorylation were considerably low, suggesting that MRLC in circular bundles as well as in stress fibres is mainly phosphorylated by Rho-kinase. The results of the immunoblotting analysis support this notion.

We have shown that when Rho-kinase or the interaction between actin and myosin-II was inhibited, neither circular bundles nor stress fibres were formed (Figs 5A and 5B), suggesting that these structures are organized in a manner dependent on myosin-II activity that is enhanced by Rho-kinase-mediated MRLC phosphorylation. When Rho-kinase was inhibited, cells initially spread to a larger extent than did the control cells (Fig. 5C). Since contractility arises from the activity of myosin-II phosphorylated by Rho-kinase, and circular bundles contain phosphorylated myosin-II, the inhibition of Rho-kinase would lead to a loss of contractility of circular bundles. Furthermore, circular bundles were destroyed when myosin-II activity was inhibited by Y-27632 or blebbistatin (Fig. 6). Therefore, isometric tension arising from the contractility is essential for the maintenance of the structure of circular bundles, and this tension appeared to restrict cell spreading because the cell area increased after the inhibitor treatments increased.

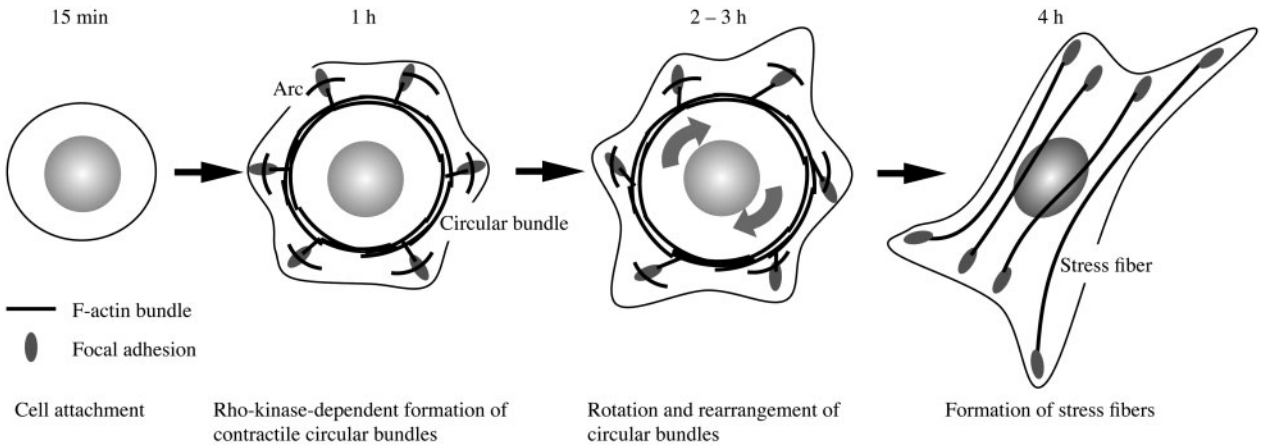

Fig. 9. **Schematic representation of the actin bundle dynamics during fibroblast spreading.** By 1 h after the plating, circular bundles and dorsal stress fibres are formed. The ends of dorsal stress fibres are attached to the substrate through focal adhesion proteins such as integrin $\alpha_v\beta_3$ and vinculin. Arcs are organized at the cell periphery, transported, joined with each other and then transformed into circular bundles with myosin-II. In circular bundles, MRLC is phosphorylated mainly by Rho-kinase. Thus, circular bundles possess the contractility that is necessary for the formation and maintenance of circular bundles. The isometric tension arising from the contractility of circular bundles must be transmitted to the underlying substrate through dorsal stress fibres whose ends are located at focal adhesions, and this tension appears as a traction force that is directed radially towards the nucleus judging from the elongated shape of focal adhesions. In this scenario, circular bundles are presumed to regulate cell morphology by inhibiting spreading. When arcs cease to flow, circular bundles begin to undergo rotation (grey arrows). After 4 h, stress fibres are formed. This process mainly depends on Rho-kinase. Organized stress fibres are static, and unlike circular bundles, do not show dynamic behaviour. Vinculin clusters are oriented in the direction of stress fibres by this time.

Other kinases, such as the MLCK, have been known to phosphorylate MRLC. Thus, we examined the effect of MLCK on circular bundles using an MLCK inhibitor, ML-7 or ML-9. However, circular bundles and stress fibres were formed in the cells incubated with 10 μM ML-7 or 30 μM ML-9 (data not shown). The possibility of decomposition of the inhibitor was remote, because the medium-containing ML-7 was replaced every 2 h after the first addition. Furthermore, increase in the ML-7 concentration up to 20 μM produced the same results. A further increase in the ML-7 concentration would cause effects other than inhibiting the phosphorylation of MLCK (*23*). Thus, MLCK-dependent MRLC phosphorylation did not appear to be necessary for the formation of circular bundles and stress fibres. However, ML-7 treatment did affect the cell morphology. The cell area was smaller at 0.5, 1, 2 and 4 h ($P < 0.01$) after the plating and the form factor was larger than that of the control cells at 15 min ($P < 0.01$), 1 h ($P < 0.05$), 2 h ($P < 0.01$), 4 h ($P < 0.01$) and 8 h ($P < 0.05$), indicating a rounder shape of the ML-7-treated cells during cell spreading. One reason for this may be the loss of the arch-shaped peripheral actin bundles that are organized from lamellipodial membrane protrusions (*9*, *12*, *46–48*). Thus, the inhibition of MLCK seems to suppress the formation of peripheral actin bundles, which induced a rounder cell shape. These results suggest that the formation of circular bundles strongly depends on Rho-kinase but not on MLCK-mediated myosin activity.

The experiments with a digitonin-permeabilized cell model that is capable of contraction provide a greater understanding of the mechanical behaviour of circular bundles (Fig. 7). Mg-ATP induced the isotropic contraction of circular bundles in a lateral direction. Traction force microscopy has previously revealed that in the early stages of cell spreading, traction force on the substrate was generated in the radial direction (*49*). Our results suggest that the origin of traction force is the isometric tension of circular bundles, which is thought to be transmitted to the substrate through dorsal stress fibres that are arranged in the radial direction. The fact that elliptical shape of vinculin clusters observed at this stage of cell spreading supports this idea, because the orientation of elongated focal adhesions generally coincides with the direction of the contractile force (*50*). In well-spread cells, the direction of the contraction and the orientation of vinculin clusters were parallel to the long axis of the cell. We suggest that the direction of the traction force changed concomitantly with the morphological changes in F-actin bundles during cell spreading, which also altered the direction of vinculin clusters.

Furthermore, when cells were partially dissociated using trypsin-EDTA in the early stages of spreading, the cells retracted and circular bundles contracted followed by complete disappearance (Fig. 8A). On the other hand, cells in which the formation of circular bundles was inhibited by Y-27632 treatment did not show a rapid retraction after partial dissociation from the substrate (Figs 8C and 8D). The cell area slowly decreased by Y-27632 treatment, but this was probably due to the effect of the tension that was developed in the membrane of the spread cell (*51*). These results suggest that circular bundles maintained their structure via the isometric tension that they develop and that the maintenance of the straight structure of stress fibres occurred similarly (*52*, *53*). These findings will offer new insight into the study of cell migration and cell adhesions as well as the study of cell spreading.

When circular bundles were restructured into stress fibres, they underwent rotation. It has been suggested that the elongating dorsal stress fibres induced this rotation (*39*). Actin polymerization of the dorsal stress fibres is known to be promoted by mDia1, an actin polymerization factor (*2*). To further understand the relationship between the elongation of dorsal stress fibres and the rotation of circular bundles, it will be necessary to investigate the role of mDia1 in spreading cells. On the other hand, it is known that the centrosome of microtubules induces the rotation of the nucleus in polarizing cells (*54*). Recent studies have shown that mDia1 regulates microtubule alignment in polarizing cells (*55–57*). It is important to understand the cooperation between mDia1 function and microtubule dynamics in spreading cells.

SUPPLEMENTARY DATA

Supplementary data are available at *JB* online.

FUNDING

Tohoku University 21COE Program 'Exploring New Science by Bridging Particle—Matter Hierarchy'.

CONFLICT OF INTEREST

None declared.

REFERENCES

1. Peterson, L.J., Rajfur, Z., Maddox, A.S., Freel, C.D., Chen, Y., Edlund, M., Otey, C., and Burridge, K. (2004) Simultaneous stretching and contraction of stress fibers in vivo. *Mol. Biol. Cell* **15**, 3497–3508
2. Hotulainen, P. and Lappalainen, P. (2006) Stress fibers are generated by two distinct actin assembly mechanisms in motile cells. *J. Cell Biol.* **173**, 383–394
3. Sanger, J.M., Mittal, B., Pochapin, M.B., and Sanger, J.W. (1987) Stress fiber and cleavage furrow formation in living cells microinjected with fluorescently labeled alpha-actinin. *Cell Motil. Cytoskeleton* **7**, 209–220
4. Edlund, M., Lotano, M.A., and Otey, C.A. (2001) Dynamics of alpha-actinin in focal adhesions and stress fibers visualized with alpha-actinin-green fluorescent protein. *Cell Motil. Cytoskeleton* **48**, 190–200
5. Ranucci, D., Yamakita, Y., Matsumura, F., and Hitchcock-DeGregori, S.E. (1993) Incorporation of microinjected mutant and wildtype recombinant tropomyosins into stress fibers in fibroblasts. *Cell Motil. Cytoskeleton* **24**, 119–128
6. Katoh, K., Kano, Y., Masuda, M., Onishi, H., and Fujiwara, K. (1998) Isolation and contraction of the stress fiber. *Mol. Biol. Cell* **9**, 1919–1938
7. Katoh, K., Kano, Y., Amano, M., Onishi, H., Kaibuchi, K., and Fujiwara, K. (2001) Rho-kinase-mediated contraction of isolated stress fibers. *J. Cell Biol.* **153**, 569–584
8. Kumar, S., Maxwell, I.Z., Heisterkamp, A., Polte, T.R., Lele, T.P., Salanga, M., Mazur, E., and Ingber, D.E. (2006) Viscoelastic retraction of single living stress fibers and its

impact on cell shape, cytoskeletal organization, and extracellular matrix mechanics. *Biophys. J.* **90**, 3762–3773
9. Small, J.V., Rottner, K., Kaverina, I., and Anderson, K.I. (1998) Assembling an actin cytoskeleton for cell attachment and movement. *Biochim. Biophys. Acta* **1404**, 271–281
10. Heath, J.P. (1983) Behaviour and structure of the leading lamella in moving fibroblasts. I. Occurrence and centripetal movement of arc-shaped microfilament bundles beneath the dorsal cell surface. *J. Cell Sci.* **60**, 331–354
11. Wang, Y.L. (1984) Reorganization of actin filament bundles in living fibroblasts. *J. Cell Biol.* **99**, 1478–1485
12. Small, J.V. and Resch, G.P. (2005) The comings and goings of actin: coupling protrusion and retraction in cell motility. *Curr. Opin. Cell. Biol.* **17**, 517–523
13. Henson, J.H., Svitkina, T.M., Burns, A.R., Hughes, H.E., MacPartland, K.J., Nazarian, R., and Borisy, G.G. (1999) Two components of actin-based retrograde flow in sea urchin coelomocytes. *Mol. Biol. Cell* **10**, 4075–4090
14. Zhang, X.F., Schaefer, A.W., Burnette, D.T., Schoonderwoert, V.T., and Forscher, P. (2003) Rho-dependent contractile responses in the neuronal growth cone are independent of classical peripheral retrograde actin flow. *Neuron* **40**, 931–944
15. Amano, M., Ito, M., Kimura, K., Fukata, Y., Chihara, K., Nakano, T., Matsuura, Y., and Kaibuchi, K. (1996) Phosphorylation and activation of myosin by Rho-associated kinase (Rho-kinase). *J. Biol. Chem.* **271**, 20246–20249
16. Ikebe, M. and Hartshorne, D.J. (1985) Phosphorylation of smooth muscle myosin at two distinct sites by myosin light chain kinase. *J. Biol. Chem.* **260**, 10027–10031
17. Kimura, K., Ito, M., Amano, M., Chihara, K., Fukata, Y., Nakafuku, M., Yamamori, B., Feng, J., Nakano, T., Okawa, K., Iwamatsu, A., and Kaibuchi, K. (1996) Regulation of myosin phosphatase by Rho and Rho-associated kinase (Rho-kinase). *Science* **273**, 245–248
18. Kawano, Y., Fukata, Y., Oshiro, N., Amano, M., Nakamura, T., Ito, M., Matsumura, F., Inagaki, M., and Kaibuchi, K. (1999) Phosphorylation of myosin-binding subunit (MBS) of myosin phosphatase by Rho-kinase in vivo. *J. Cell Biol.* **147**, 1023–1038
19. Vasiliev, J.M. (1985) Spreading of non-transformed and transformed cells. *Biochim. Biophys. Acta* **780**, 21–65
20. Heath, J.P. and Holifield, B.F. (1993) On the mechanisms of cortical actin flow and its role in cytoskeletal organisation of fibroblasts. *Symp. Soc. Exp. Biol.* **47**, 35–56
21. Hirata, H., Ohki, K., and Miyata, H. (2003) Change of the topography of ventral, cell surface during spreading of fibroblasts as revealed by evanescent wave-excited fluorescence microscopy: effect of contractility and microtubule integrity. *JSME Int. J. Ser. C* **46**, 1208–1217
22. Uehata, M., Ishizaki, T., Satoh, H., Ono, T., Kawahara, T., Morishita, T., Tamakawa, H., Yamagami, K., Inui, J., Maekawa, M., and Narumiya, S. (1997) Calcium sensitization of smooth muscle mediated by a Rho-associated protein kinase in hypertension. *Nature* **389**, 990–994
23. Saitoh, M., Ishikawa, T., Matsushima, S., Naka, M., and Hidaka, H. (1987) Selective inhibition of catalytic activity of smooth muscle myosin light chain kinase. *J. Biol. Chem.* **262**, 7796–7801
24. Straight, A.F., Cheung, A., Limouze, J., Chen, I., Westwood, N.J., Sellers, J.R., and Mitchison, T.J. (2003) Dissecting temporal and spatial control of cytokinesis with a myosin II Inhibitor. *Science* **299**, 1743–1747
25. Kolega, J. (2004) Phototoxicity and photoinactivation of blebbistatin in UV and visible light. *Biochem. Biophys. Res. Commun.* **320**, 1020–1025
26. Sakamoto, T., Limouze, J., Combs, C.A., Straight, A.F., and Sellers, J.R. (2005) Blebbistatin, a myosin II inhibitor, is photoinactivated by blue light. *Biochemistry* **44**, 584–588
27. Watanabe, T., Hosoya, H., and Yonemura, S. (2006) Regulation of myosin II dynamics by phosphorylation and dephosphorylation of its light chain in epithelial cells. *Mol. Biol. Cell* **18**, 605–616
28. Laemmli, U.K. (1970) Cleavage of structural proteins during the assembly of the head of bacteriophage T4. *Nature* **227**, 680–685
29. Owaribe, K. and Masuda, H. (1982) Isolation and characterization of circumferential microfilament bundles from retinal pigmented epithelial cells. *J. Cell Biol.* **95**, 310–315
30. Hirata, H., Tatsumi, H., and Sokabe, M. (2004) Tension-dependent formation of stress fibers in fibroblasts: a study using semi-intact cells. *JSME Int. J. Ser. C* **47**, 962–969
31. Conrad, P.A., Giuliano, K.A., Fisher, G., Collins, K., Matsudaira, P.T., and Taylor, D.L. (1993) Relative distribution of actin, myosin I, and myosin II during the wound healing response of fibroblasts. *J. Cell Biol.* **120**, 1381–1391
32. Small, J.V. and Celis, J.E. (1978) Filament arrangements in negatively stained cultured cells: the organization of actin. *Cytobiologie* **16**, 308–325
33. Altankov, G. and Grinnell, F. (1993) Depletion of intracellular potassium disrupts coated pits and reversibly inhibits cell polarization during fibroblast spreading. *J. Cell Biol.* **120**, 1449–1459
34. McKenna, N.M., Wang, Y.L., and Konkel, M.E. (1989) Formation and movement of myosin-containing structures in living fibroblasts. *J. Cell Biol.* **109**, 1163–1172
35. Cramer, L.P. and Mitchison, T.J. (1995) Myosin is involved in postmitotic cell spreading. *J. Cell Biol.* **131**, 179–189
36. Verkhovsky, A.B., Svitkina, T.M., and Borisy, G.G. (1995) Myosin II filament assemblies in the active lamella of fibroblasts: their morphogenesis and role in the formation of actin filament bundles. *J. Cell Biol.* **131**, 989–1002
37. Gupton, S.L., Anderson, K.L., Kole, T.P., Fischer, R.S., Ponti, A., Hitchcock-DeGregori, S.E., Danuser, G., Fowler, V.M., Wirtz, D., Hanein, D., and Waterman-Storer, C.M. (2005) Cell migration without a lamellipodium: translation of actin dynamics into cell movement mediated by tropomyosin. *J. Cell Biol.* **168**, 619–631
38. Zamir, E., Katz, M., Posen, Y., Erez, N., Yamada, K.M., Katz, B.Z., Lin, S., Lin, D.C., Bershadsky, A., Kam, Z., and Geiger, B. (2000) Dynamics and segregation of cell-matrix adhesions in cultured fibroblasts. *Nat. Cell Biol.* **2**, 191–196
39. Soranno, T. and Bell, E. (1982) Cytostructural dynamics of spreading and translocating cells. *J. Cell Biol.* **95**, 127–136
40. Ueda, K., Murata-Hori, M., Tatsuka, M., and Hosoya, H. (2002) Rho-kinase contributes to diphosphorylation of myosin II regulatory light chain in nonmuscle cells. *Oncogene* **21**, 5852–5860
41. Chrzanowska-Wodnicka, M. and Burridge, K. (1996) Rho-stimulated contractility drives the formation of stress fibers and focal adhesions. *J. Cell Biol.* **133**, 1403–1415
42. Burridge, K., Fath, K., Kelly, T., Nuckolls, G., and Turner, C. (1988) Focal adhesions: transmembrane junctions between the extracellular matrix and the cytoskeleton. *Annu. Rev. Cell Biol.* **4**, 487–525
43. Chen, W.T. (1981) Mechanism of retraction of the trailing edge during fibroblast movement. *J. Cell Biol.* **90**, 187–200
44. Thoumine, O. and Ott, A. (1996) Influence of adhesion and cytoskeletal integrity on fibroblast traction. *Cell Motil. Cytoskeleton* **35**, 269–280
45. Badley, R.A., Woods, A., Carruthers, L., and Rees, D.A. (1980) Cytoskeleton changes in fibroblast adhesion and detachment. *J. Cell Sci.* **43**, 379–390
46. Totsukawa, G., Yamakita, Y., Yamashiro, S., Hartshorne, D.J., Sasaki, Y., and Matsumura, F. (2000) Distinct roles of ROCK (Rho-kinase) and MLCK in spatial regulation of MLC phosphorylation for assembly of stress fibers and focal adhesions in 3T3 fibroblasts. *J. Cell Biol.* **150**, 797–806
47. Katoh, K., Kano, Y., Amano, M., Kaibuchi, K., and Fujiwara, K. (2001) Stress fiber organization regulated by

MLCK and Rho-kinase in cultured human fibroblasts. *Am. J. Physiol. Cell Physiol.* **280**, C1669–C1679
48. Yanase, M., Ikeda, H., Ogata, I., Matsui, A., Noiri, E., Tomiya, T., Arai, M., Inoue, Y., Tejima, K., Nagashima, K., Nishikawa, T., Shibata, M., Ikebe, M., Rojkind, M., and Fujiwara, K. (2003) Functional diversity between Rho-kinase- and MLCK-mediated cytoskeletal actions in a myofibroblast-like hepatic stellate cell line. *Biochem. Biophys. Res. Commun.* **305**, 223–228
49. Reinhart-King, C.A., Dembo, M., and Hammer, D.A. (2005) The dynamics and mechanics of endothelial cell spreading. *Biophys. J.* **89**, 676–689
50. Balaban, N.Q., Schwarz, U.S., Riveline, D., Goichberg, P., Tzur, G., Sabanay, I., Mahalu, D., Safran, S., Bershadsky, A., Addadi, L., and Geiger, B. (2001) Force and focal adhesion assembly: a close relationship studied using elastic micropatterned substrates. *Nat. Cell Biol.* **3**, 466–472
51. Albrecht-Buehler, G. (1987) Role of cortical tension in fibroblast shape and movement. *Cell Motil. Cytoskeleton* **7**, 54–67
52. Ingber, D.E. (2003) Tensegrity I. Cell structure and hierarchical systems biology. *J. Cell Sci.* **116**, 1157–1173
53. Ingber, D.E. (2003) Tensegrity II. How structural networks influence cellular information processing networks. *J. Cell Sci.* **116**, 1397–1408
54. Waterman-Storer, C.M., Worthylake, R.A., Liu, B.P., Burridge, K., and Salmon, E.D. (1999) Microtubule growth activates Rac1 to promote lamellipodial protrusion in fibroblasts. *Nat. Cell Biol.* **1**, 45–50
55. Ishizaki, T., Morishima, Y., Okamoto, M., Furuyashiki, T., Kato, T., and Narumiya, S. (2001) Coordination of microtubules and the actin cytoskeleton by the Rho effector mDia1. *Nat. Cell Biol.* **3**, 8–14
56. Palazzo, A.F., Cook, T.A., Alberts, A.S., and Gundersen, G.G. (2001) mDia mediates Rho-regulated formation and orientation of stable microtubules. *Nat. Cell Biol.* **3**, 723–729
57. Yamana, N., Arakawa, Y., Nishino, T., Kurokawa, K., Tanji, M., Itoh, R.E., Monypenny, J., Ishizaki, T., Bito, H., Nozaki, K., Hashimoto, N., Matsuda, M., and Narumiya, S. (2006) The Rho-mDia1 pathway regulates cell polarity and focal adhesion turnover in migrating cells through mobilizing Apc and c-Src. *Mol. Cell Biol.* **26**, 6844–6858